Determination of laminar burning characteristics of a surrogate for a pyrolysis fuel using constant volume method

Xu, C., Wang, H., Oppong, F., Li, X., Zhou, K., Zhou, W., Wu, S. & Wang, C.

Original citation & hyperlink:
Xu, C, Wang, H, Oppong, F, Li, X, Zhou, K, Zhou, W, Wu, S & Wang, C 2020, 'Determination of laminar burning characteristics of a surrogate for a pyrolysis fuel using constant volume method', Energy, vol. 190, 116315.
https://dx.doi.org/10.1016/j.energy.2019.116315

DOI 10.1016/j.energy.2019.116315
ISSN 0360-5442

Publisher: Elsevier

Determination of laminar burning characteristics of a surrogate for a pyrolysis fuel using constant volume method

Cangsu Xu[a], *Hanyu Wang*[a], *Francis Oppong*[a], *Xiaolu Li*[b],

Kangquan Zhou[a], *Wenhua Zhou*[a], *SiyuanWu*[a], *Chongming Wang*[c*]

[a] *College of Energy Engineering, Zhejiang University, Hangzhou, China, 310027*

[b] *College of Mechanical and Electrical Engineering, China Jiliang University, Hangzhou, China, 310018*

[c] *School of Mechanical, Aerospace and Automotive Engineering, Coventry University, Coventry, United Kingdom, CV1 5FB*

[*] Corresponding author *e-mail address*: ac8174@coventry.ac.uk

Abstract

A fast pyrolysis biofuel, mainly consisting to 98% of ethanol, ethyl acetate, diethyl ether, acetone and 2-butanone with mass ratios of 9:6:2:1:1, was catalytically produced from rice husk. A preliminary engine test demonstrated this biofuel has the possibility of being a gasoline blending stock. However, its fundamental burning features are not fully understood. This work presents the experimental investigations of the spherical propagating flame of a surrogate fuel representing the biofuel in a constant volume combustion chamber (CVCC). Tests were conducted at initial pressures of 0.1-0.4 MPa, initial temperatures of 358-418 K, and equivalence ratios of 0.7-1.4. Employing the constant volume method (CVM) allows determining laminar burning speeds (S_u) of this surrogate at conditions far beyond the initial conditions (0.1-0.8 MPa, 358-490 K). Power law fitting correlations between S_u and pressure were obtained via the constant volume method (CVM). Cellularity appears when pressure or temperature is high, and cellular burning speed was calculated by CVM as well. S_u determined via the constant pressure method (CPM) were compared with those from the CVM. Discrepancies between the results from the CVM and the CPM are within 15%, except at the conditions where flame cellularity appeared. Additionally, an explicit correlation of S_u was obtained from the experimental results.

Keywords: biofuel; laminar burning speed; constant-volume method; cellular flame speed

Greek symbols

ϕ	Equivalence ratio
ρ_i	Initial density (kg/m^3)
ρ_u	Density of unburned gas (kg/m^3)
κ	Stretch rate (s^{-1})
α	Temperature exponent
β	Pressure exponent

Symbols

S_u^0	Laminar burning speed at initial condition (m/s)
S_u	Laminar burning speed obtained by CVM (m/s)
$S_{u,CPM}$	Laminar burning speed obtained by CPM (m/s)
S_g	Expansion speed of burned gas (m/s)
S_f	Flame front propagation speed (m/s)
p	Combustion pressure (MPa)
p_i	Initial pressure (MPa)
p_e	Peak pressure (MPa)
T_u	Unburned gas temperature (K)
T_i	Initial gas temperature (K)
x	Burned mass fraction
p_r	Pressure rise fraction
m_i	Mass of initial gas (kg)
m_u	Mass of unburned gas (kg)
m_b	Mass of burned gas (kg)
r_f	Radius of flame front (m)
r_w	Radius of combustion chamber (m)
A_f	Area of flame front (m^2)
k_u	Heat capacity ratio of unburned gas

$C_{p,u}$	Molar heat capacity of unburned gas at constant pressure (J/(mol•K))
$C_{p,j}$	Molar heat capacity of *j* component at constant pressure (J/(mol•K))
$C_{p,air}$	Molar heat capacity of air at constant pressure (J/(mol•K))
$C_{v,u}$	Molar heat capacity of unburned gas at constant volume (J/(mol•K))
a_j	Volumetric air-fuel ratio of *j* component
n_j	Molar fraction of *j* component
R_g	Gas constant

Subscripts

u	Unburned gas
b	Burned gas
i	Initial condition
j	*j* component in the mixture

1 Introduction

Clean renewable energy resources, for example, biomass, are mid- and long-term solutions for the depletion of fossil fuels and environmental pollution [1]. Fast pyrolysis biofuel is considered as one of the promising alternative fuels. Recently, a fast pyrolysis biofuel was produced from rice husk at Zhejiang University [2,3]. Based on detailed composition analysis of that biofuel, a mixed fuel which consists of ethanol, ethyl acetate, diethyl ether, acetone and 2-butanone with mass ratios of 9:6:2:1:1, can be used as a surrogate for this biofuel [3,4].

Laminar burning speed (S_u) is the velocity where one-dimensional, planar, adiabatic, un-stretched [5,6] and premixed flame propagates through the unburned gas mixture. It is an essential intrinsic parameter of a combustible mixture [7-12]. S_u helps to explain combustion phenomena, such as extinction [13-15], flashback, and blow off [16,17]. It also conveys information about diffusivity, reactivity, and exothermicity of the combustible mixture [18]. Therefore, it is important for designing practical combustion systems [19-22], especially at temperatures and pressures higher than the ambient condition. Moreover, it is an essential input parameter for turbulent combustion models [23,24].

There are many experimental setups for identifying S_u, including the Bunsen flame, counter-flow flame, flat flame and constant volume combustion chamber (CVCC). CVCC is the most commonly used [21,22,25]. There are two different ways to obtain S_u in the CVCC, the constant pressure method (CPM) and the constant volume method (CVM). The CPM was first announced by Ellis [26] in 1928, while the CVM was initially mentioned by Lewis and von Elbe in 1934 [27]. In the CPM, CVCC is set up in the Schlieren system, and a high-speed camera records Schlieren images [4], from which the quasi-steady smooth spherical flame in early propagation period is chosen for data analysis [27]. Meanwhile, the flame structure can be observed in the Schlieren photographs to determine when flame cellularity and instability occur. In the CVM, combustion pressure is recorded, and S_u is calculated as the function of pressure (p) and burned gas fraction (x) [27]. S_u calculated via the CVM involves a few assumptions; therefore, it tends to be less accurate than that obtained from the CPM. However, there are two remarkable advantages that make CVM indispensable. Firstly, for a given mixture, S_u can be continuously obtained over a wide range of pressures and temperatures from a single experiment [10,28]. Thus, S_u at higher pressures and temperatures close to practical engine operating conditions (3-7 MPa and 700-800 K) can be obtained. In addition, cellular flame speed can be calculated from the CVM, which cannot be determined from the CPM [29].

Several investigations have been conducted in the literature to calculate S_u using the CVM. Lewis and Von Elbe [27] proposed the widely used CVM linear x-p relation, and they used it to determine S_u. O'Donovan and Rallis [30] simplified the x-p relation by introducing the temperature gradient. Saeed

and Stone [31,32] used the multiple burned gas zone model to determine S_u. They proposed a 9-term correlation for determining S_u. Based on the multi-zone modelling, Luijten et al. [33,34] developed an alternative analytical *x-p* relation and compared it with 1D unsteady simulation and numerical two-zone model. Faghih and Chen [10] evaluated the accuracy of the various *x-p* relations used in CVM, from which it can be found that linear *x-p* relation is a reasonable choice. Chen et al. [35,36] studied the S_u of outwardly propagating spherical flames and investigated the effects of confinement, stretch, radiation and ignition energy on S_u. Huang et al. [37-39] investigated S_u of several fuels, such as dimethyl ether, natural gas–hydrogen and methanol–nitrogen/carbon dioxide at different temperatures, pressures, equivalence ratios and mentioned the appearance of cellularity. Recently, Hinton and Stone [40,41] used both CPM and CVM to investigate the S_u of aqueous ethanol and proposed an explicit 14-terms correlation for S_u as a function of pressure, temperature and equivalence ratio.

This paper investigates the spherically expanding flame of the fast pyrolysis fuel in the CVCC at initial pressures of 0.1-0.4 MPa, initial temperature of 358-418 K, and at equivalence ratios (ϕ) of 0.7-1.4. The novelty of this paper is that the CVM, which takes the combustion pressure trace as the main input, was used to determine S_u of the biofuel fast pyrolysis blend at conditions (pressure up to 0.8 MPa; temperature up to 490 K) beyond the initial conditions (pressure up to 0.4 MPa; temperature up to 418 K).

2 Experimental setup and procedures

Figure 1 provides the experimental layout with a CVCC of 1.94L inner volume. The CVCC was heated by six heating elements fitted on its walls. Moreover, ignition of the mixture was done with two electrodes (d=0.4 mm) facing each other together with ignition control set. The spark energy was maintained at 15 mJ. The spherically expanding flame images were obtained by the Schlieren imaging arrangement together with a high-speed camera (6000 fps @ 512×512 pixels) via see-through openings (Φ=105 mm) at both ends of the chamber. Combustion pressure was measured by pressure transducers, meanwhile, the experiments were done at initial temperatures of 358-418 K, initial pressures of 0.1-0.4 MPa, and equivalence ratios of 0.7-1.4. The mixture was unable to ignite at the equivalence ratio of 0.5 during our experiment, however, at the equivalence ratio of 0.6 almost 10 experiments were done and only 2-3 experiments were able to ignite the mixture. Therefore, we chose 0.7 as the lower limit for the study. On the other hand, at very rich mixtures, thus equivalence ratios beyond 1.4 the flame was unstable; hence, we chose 1.4 as the upper limit for the study. A total of 216 experiments were performed and each test was repeated three times. Complete information about the experimental

process can be found in ref. [4,42-44].

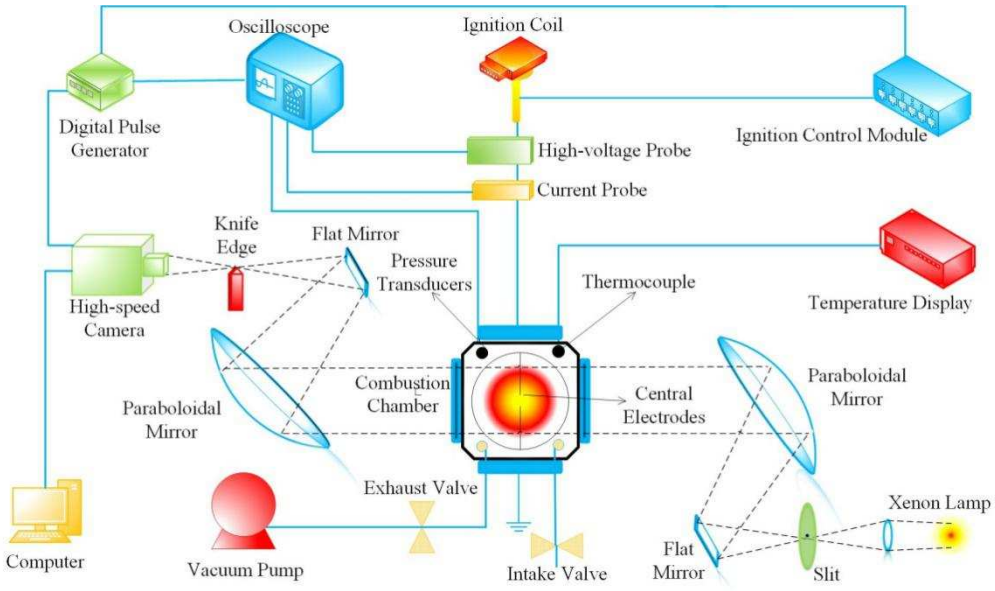

Figure 1. Experimental layout

3 Determination of S_u with CVM

There are a few assumptions for determining S_u using the CVM [10,33,40]: (1) the unburned gas is uniform, and it is compressed isentropically; (2) the pressure is uniform in the whole combustion chamber; (3) both the unburned and burned gases are ideal gas; (4) the total mass and volume of the vessel contents are conserved; (5) the external heat input, heat losses, radiation and buoyancy effects are negligible; (6) the flame stretch is negligible for large flame radius.

S_u is defined as [27]:

$$S_u = -\frac{1}{A_f \rho_u}\frac{dm_u}{dt} \tag{1}$$

where $m_u = 4(r_w^3 - r_f^3)\pi\rho_u/3$, m_u is the mass of unburned gases; ρ_u is the unburned gas density; r_f and r_w are the radius of the flame front and the CVCC. A_f is the flame front area, $A_f = 4\pi r_f^2$.

In consideration with the aforementioned assumptions, the unburned gas temperature and ρ_u can be estimated by the following equations:

$$\frac{T_u}{T_i} = \left(\frac{p}{p_i}\right)^{\frac{k_u - 1}{k_u}} \tag{2}$$

$$\frac{\rho_u}{\rho_i} = \left(\frac{p}{p_i}\right)^{\frac{1}{k_u}} \tag{3}$$

where T_u and p are the temperatures of the unburned gas and pressure in the CVCC during combustion, respectively; T_i (initial temperature), p_i (initial pressure), ρ_i (initial density) and k_u (specific heat ratio).

The burned mass fraction x, defined as the ratio of burned gas and the total amount of gas is calculated via:

$$m_u = m_i - m_b = (1 - x)m_i \tag{4}$$

where $m_i = 4\pi r_w^3 \rho_i / 3$. m_i and m_b are the mass of the initial and burned gases, respectively.

A linear relation between p and x, proposed by Lewis and von Elbe [27], can be used to estimate the burned mass fraction:

$$x = \frac{p - p_i}{p_e - p_i} \tag{5}$$

where p_e is the maximum pressure during combustion.

Combining Equations 1-4 yields [10,45]:

$$S_u = \frac{r_w}{3}\left[1 - (1 - x)\left(\frac{p_i}{p}\right)^{\frac{1}{k_u}}\right]^{-\frac{2}{3}}\left(\frac{p_i}{p}\right)^{\frac{1}{k_u}}\frac{dx}{dt} \tag{6}$$

In the linear x-p relation, the burned mass fraction x equals to the pressure rise fraction p_r [33]:

$$p_r = \frac{p - p_i}{p_e - p_i} \tag{7}$$

Five components were used as a surrogate for the fast pyrolysis fuel. Some properties of the five components are listed in Table 1. The fuel is metered by a syringe with a resolution of 1μL. Filtered workshop air is used in the combustion.

Table 1 Properties of components in fast pyrolysis fuel

Components	Ethanol	Ethyl acetate	Diethyl ether	Acetone	2-butanone
Formula	C_2H_5OH	$C_4H_8O_2$	$C_4H_{10}O$	C_3H_6O	C_4H_8O
Molecular weight (g/mol)	46.07	88.11	74.12	58.08	72.11
Weight fraction (wt.%)	47.4%	31.6%	10.5%	5.3%	5.3%
Molar fraction (mol.%)	60.7%	21.1%	8.4%	5.4%	4.3%
Volumetric air-fuel ratio	3	5	6	4	5.5

Eq. (8) was used to calculate the heat of unburned gas capacity at constant pressure. $C_{p,u}$ is an average value of specific heat capacity of ethanol, ethyl acetate, diethyl ether, acetone, 2-butanone and air with their molar fractions.

$$C_{p,u} = \frac{\varphi\sum_{j=1}^{5} C_{p,j}\cdot n_j + (\sum_{j=1}^{5} a_j \cdot n_j) C_{p,air}}{\varphi\sum_{j=1}^{5} n_j + \sum_{j=1}^{5} a_j \cdot n_j} \tag{8}$$

where a_j and n_j are the volumetric air-fuel ratio and molar fraction of each component, respectively.

To extrapolate S_u back to the initial condition, the power law correlation is used to fit the S_u [10,45]:

$$S_u = S_u^{\,0}(\frac{T}{T_i})^{\alpha}(\frac{p}{p_i})^{\beta} \tag{9}$$

where α and β are exponents of temperature and pressure, respectively. $S_u^{\,0}$ is the laminar flame speed at the initial condition and varies in different experiments.

It is assumed that the compression of unburned gas in the CVCC is adiabatic and isentropic:

$$S_u = S_u^{\,0}(\frac{p}{p_i})^{c} \tag{10}$$

where $c = \alpha((k_u - 1)/k_u) + \beta$.

4 Experimental uncertainties

The experimental uncertainties are mainly related to T_0 (ΔU_T), p_0 (ΔU_p), the flame front total inner pixels (ΔU_A), the chamber effective volume (ΔU_V) and the fuel metering (ΔU_F). ΔU_T inaccuracy is due to the thermocouple accuracy (±0.5%). Therefore, this generated errors in the estimation of the amount

of fuel injection using temperature, CVCC volume and the chosen equivalence ratio. According to the experience from authors, this is likely to generate 0.8% and 1.5% error in the estimation of the laminar burning velocity at 0.1 MPa and 0.4 MPa. The p_0 uncertainty caused less than 0.1% because the pressure sensor is accurate to 0.0001 MPa. On one hand, the flame front area uncertainty is nearly ±10 pixels, leading to almost 1% incertitude of the flame front inner pixels. ΔU_V uncertainty was almost 0.2%. The uncertainty of fuel metering relies on the capacity of fuel required for a specific test condition. In short, the CPM global uncertainty ($\sqrt{\Delta U_T^2 + \Delta U_p^2 + \Delta U_A^2 + \Delta U_V^2 + \Delta U_F^2}$) is within 2%, and that of the CVM ($\sqrt{\Delta U_T^2 + \Delta U_p^2 + \Delta U_V^2 + \Delta U_F^2}$) is about 1.5%.

5 Results and discussion

5.1. S_u determination with CVM

The temporal pressure was recorded in the experiments. Then, the first derivative (dp/dt) and the second derivative (d^2p/dt^2) of pressure were obtained. Gaussian filter was used to smooth the curve of p and dp/dt. Next, x and S_u can be calculated by eqs. (5) and (6). p_r in the range of 0.05 and 0.2 was used for determination of S_u [45]. Finally, the experimental curve of S_u in the chosen range was fitted by eq. (10).

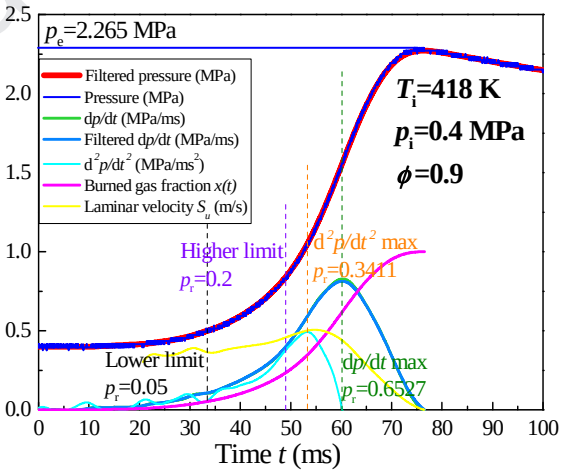

Figure 2. p, dp/dt, d^2p/dt^2, S_u and x as a function of time (initial condition: p_i= 0.4 MPa; T_i= 418 K; and ϕ=0.9).

Figure 2 shows the variation of p, dp/dt, d^2p/dt^2, x, S_u in a single experiment at the initial condition of p_i= 0.4 MPa; T_i= 418 K; and ϕ=0.9. In fact, every experiment led to a figure like Figure 2. Figure 2

is used as an example to show the profile of the main parameters. For choosing the valid calculation window, the lower limit of p_r is 0.05. There are two reasons. One is because of interference signal, so dp/dt cannot be accurately determined lower than p_r=0.05, another is because when p_r>0.05, stretch impacts can be considered negligible [45]. The higher limit is p_r=0.2, because after this point thermal loss from burned gas to the CVCC wall is non-negligible [45].

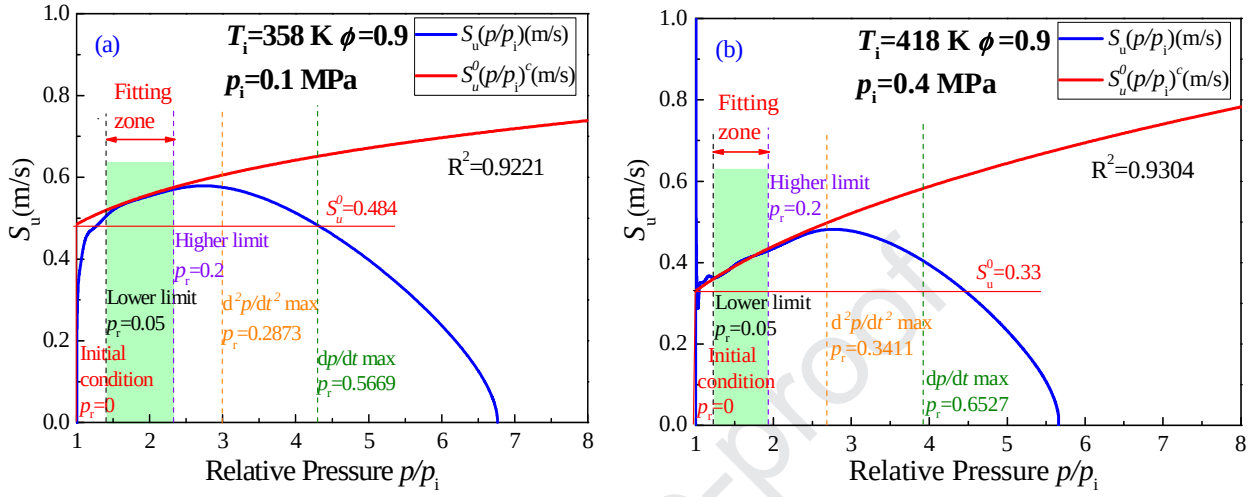

Figure 3. Graph of S_u against p/p_i at: (a) p_i= 0.1 MPa, T_i= 358 K, and ϕ=0.9; (b) p_i= 0.4 MPa, T_i= 418 K, and ϕ=0.9 (Blue lines are experimental results, while red lines are fitting correlations).

Figure 3 shows S_u at two initial conditions. The blue lines represent the experimental S_u as a function of p/p_i, whereas the red lines indicate the fitting correlations, showing just how the power law correlation was used for fitting S_u and again extrapolated to the initial and higher conditions. The experimental S_u increases with the relative pressure at first and then decreases. During the combustion procedure, the pressure and temperature increase simultaneously. At the early stage, S_u increases with increasing pressure and temperature. At relative pressure of 1, a very steep rise appears because of spark effects on combustion onset, numerical oscillations and stretch effects [46]. However, when pressure exceeds a certain value (such as p_r > 0.3411@ initial condition of $p_{i=}$ 0.4 MPa; T_i= 418 K; and ϕ=0.9), the heat loss becomes significant, which slows down the pressure rise and S_u decreases at the last stage. As mentioned earlier in Section 4.1, the fitting zone is p_r =0.05-0.2 and eq. (10) was used to fit S_u from the experiments. The coefficients, c and S_u^0 in eq. (10), were obtained for all conditions. S_u was extrapolated at the initial condition. At the initial condition, p_r is 0. According to the fitting results between the experimental lines and fitting lines, p/p_i =2 is the last point where experimental lines and fitting lines fit well for the most conditions in this study. Therefore, S_u from p/p_i =1 to p/p_i =2 were used in this paper.

5.2. Comparison of S_u obtained from CPM and CVM

Figure 4(a) compares S_u obtained from the CVM and CPM at T_i=358 K and p_i=0.1, 0.2, 0.4 MPa. The red lines represent results from the CVM while the blue lines are the CPM data. It can be found that CVM results are larger than results from the CPM. The maximum flame speed always occurs near ϕ=1.1. Further, as the pressure rises, the peak S_u shifts towards the higher equivalence ratio. With pressure increasing, S_u decreases, except the conditions for which cellularity appears. Figure 4(b) compares the results at p_i=0.1 MPa and T_i=358, 388, 418 K.

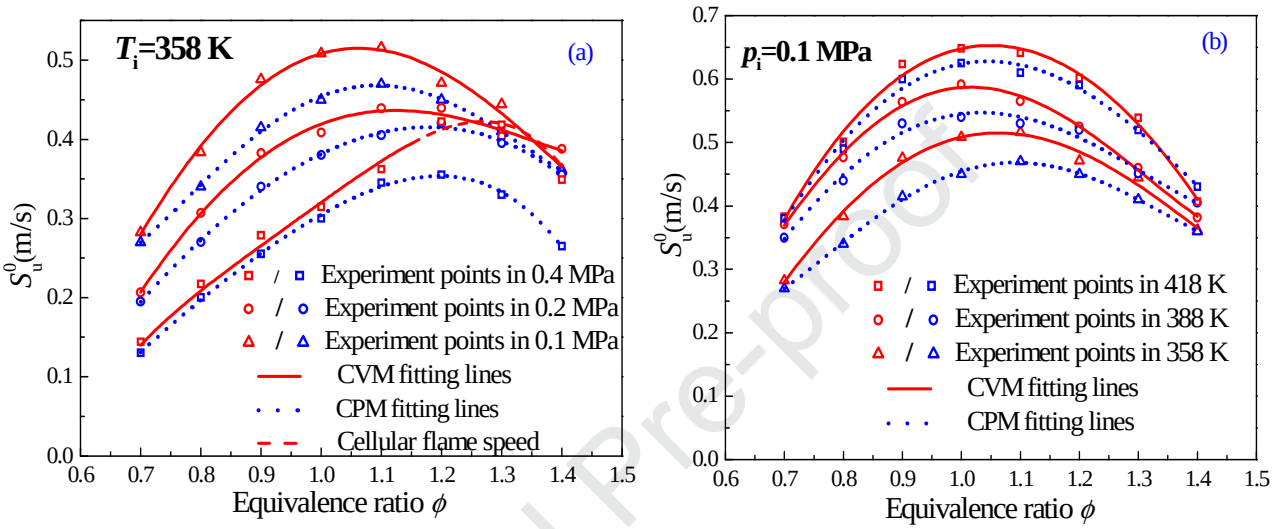

Figure 4. S_u as a function of ϕ at the conditions of: (a) p_i= 0.1, 0.2 and 0.4 MPa; T_i= 358 K; (b) p_i= 0.1 MPa; T_i= 358, 388 and 418 K (Red solid lines and red symbols are results from the CVM, while blue dotted lines and blue symbols are from the CPM. Dash line show cellular flame speed).

Figure 5 shows the relative deviation in S_u between the CVM and the CPM. The relative deviation is $(S_u - S_{u,CPM})/S_{u.CPM}$ *100%. It can be seen that the relative deviations are within 15% except for the conditions that cellularity occurs which led to a large increase in flame speed. Omari et al. [45] showed S_u data from the linear x-p relation was 20% higher when compared to the CPM. Moreover, values of CVM are consistently larger than those of CPM except for the conditions where p_i=0.1 MPa, T_i=388 and 418 K, and ϕ=1.4. On the other hand, the flame radius calculation in the CPM involves errors; therefore, it also contributes to the discrepancy in S_u between the CVM and the CPM. Overall, S_u obtained from the CVM is larger than that from the CPM in most cases.

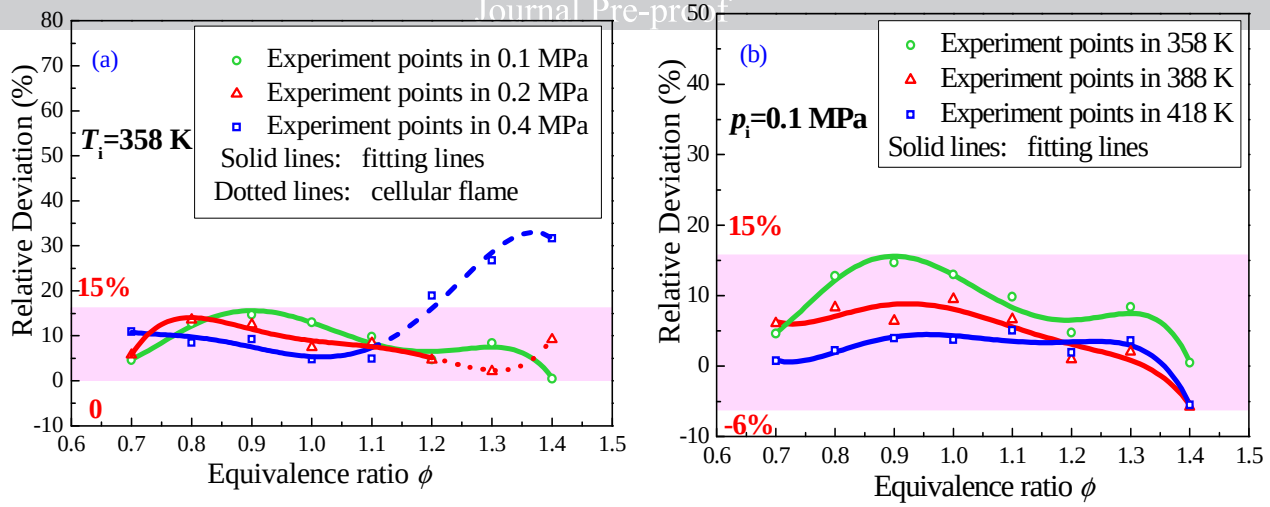

Figure 5. Relative deviation in S_u^0 obtained from the CVM and CPM at the conditions of: (a) T_i=358 K, p_i=0.1, 0.2 and 0.4 MPa; (b) p_i=0.1 MPa, T_i=358, 388 and 418 K (Solid lines refer to the relative error of S_u^0, while dotted lines indicate relative error of cellular flame speed. The shadow areas represent error ranges).

Figure 6 is used as an example to show the condition where cellularity appears. The flame speed rises rapidly as well as the fitting line. So, this indicates why the cellular flame speed is considerable larger than S_u in CPM as disclosed at the conditions where the T_i=358 K, p_i=0.4 MPa and ϕ=1.2-1.4 in Figure 4. The equivalence ratios which correspond to the appearance of cellularity are listed in Table 2.

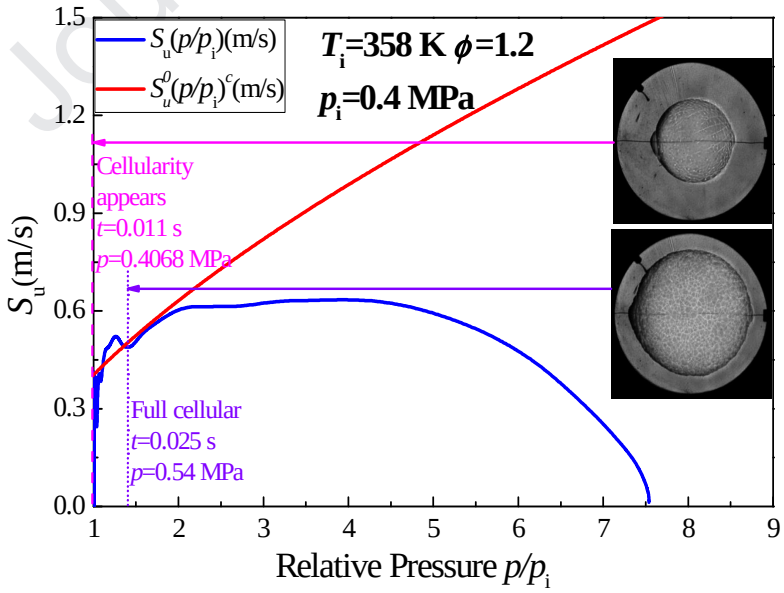

Figure 6. A graph of S_u versus p/p_i at p_i=0.4 MPa, T_i=358 K, and ϕ=1.2. (Blue line is from experiment, and red line is from fitting correlation).

Table 2 Minimum equivalence ratio for which cellularity appears

p_i \T_i	358 K	388 K	418 K
0.1 MPa	none	none	none
0.2 MPa	1.3	1.3	1.3
0.4 MPa	1.2	1.2	1.2

5.3. Impact of pressure on S_u^0

Figure 7 shows the impact of p on S_u^0 at T_i =358, 388 and 418 K. S_u^0 decreases as pressure increases. Flame cellularity tends to occur in the rich flames, caused by hydrodynamic instability. Flame cellularity accelerates flame speed, which causes S_u^0 to increase with the increase of pressure at ϕ=1.2-1.4. The phenomenon is not obvious at T_i=358 K, but when T_i=388 and 418 K, it becomes apparent. Uncertainties from preparation using CVM in the experiments is 1.5%. And uncertainties from measurement using CVM in the experiments are 0 - 2%. Error bars drawn in Figure 7 can show the uncertainties from the measurement.

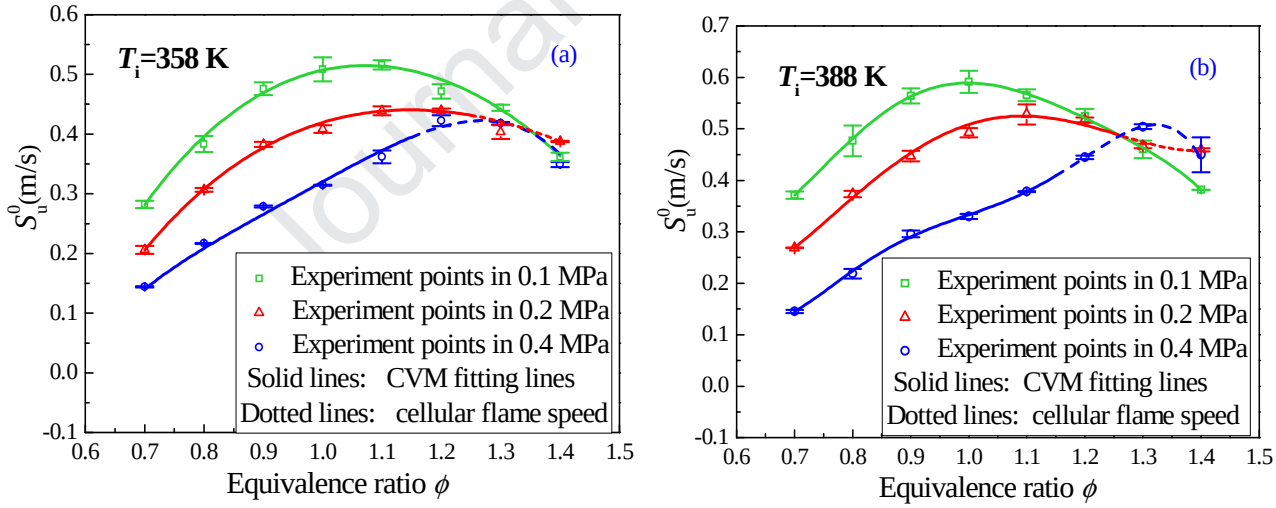

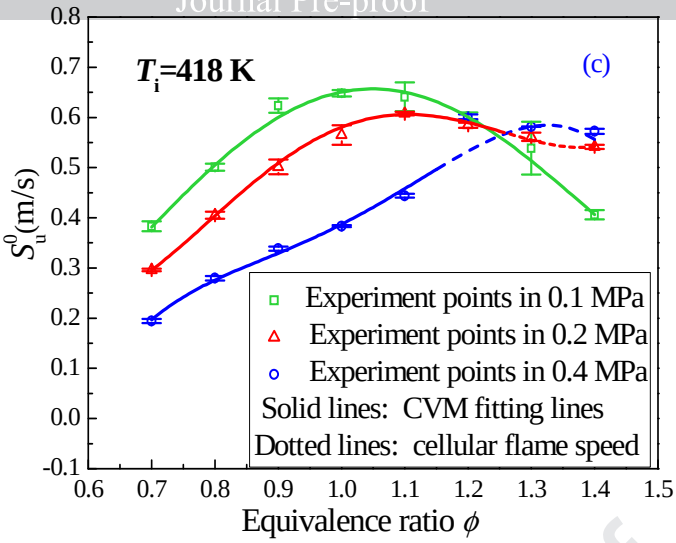

Figure 7. Impact of p on S_u^0 (a) T_i=358 K; (b) T_i =388 K; (c) T_i =418 K. (Solid lines stand for S_u^0, while dotted lines stand for cellular flame speed).

Figure 8 shows S_u as a function of p at ϕ=0.7-1.4 and T_i=358, 388 and 418 K. The power law correlations fitted to p_i=0.1, 0.2 and 0.4 MPa give a very good fit. According to the fitting zone referred in Section 4.1, S_u could be obtained at p=0.8 MPa. It can be seen from Figure 8 that S_u decreases with an increase in pressure except for the conditions for which ϕ=1.2-1.4. It is obvious that when the equivalence radio is increased from 1.2 to 1.4, the tendency of S_u is different from the others, even when ϕ=1.3-1.4, they increase as the pressure increases. The reason is that cellularity occurs when ϕ=1.2-1.4, which causes the flame speed to be larger than the value it should be and flame speeds at elevated pressure are higher than that at atmospheric pressure.

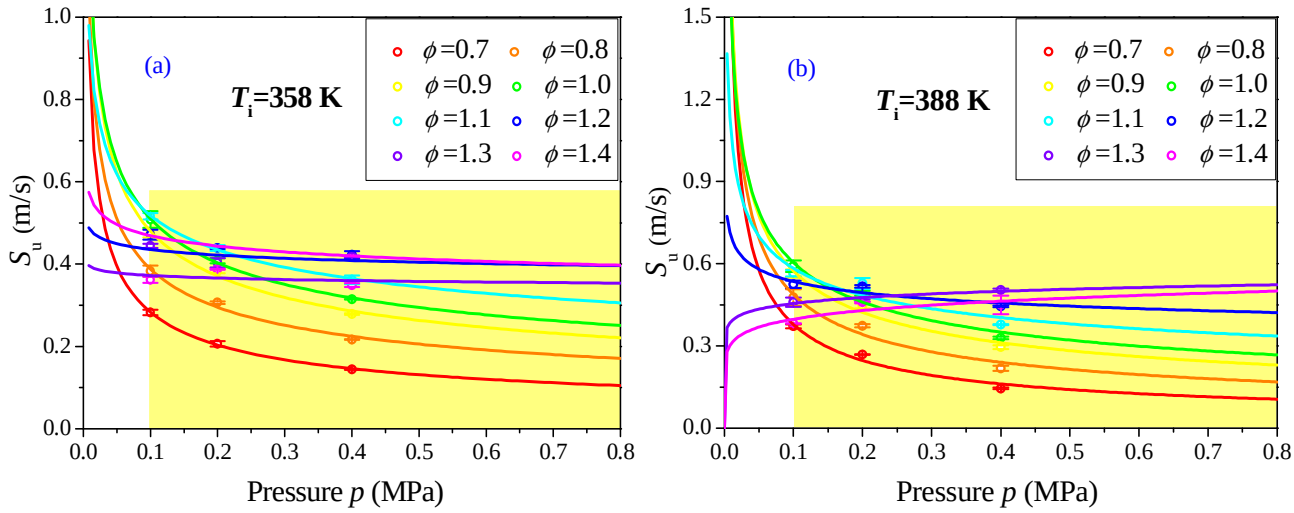

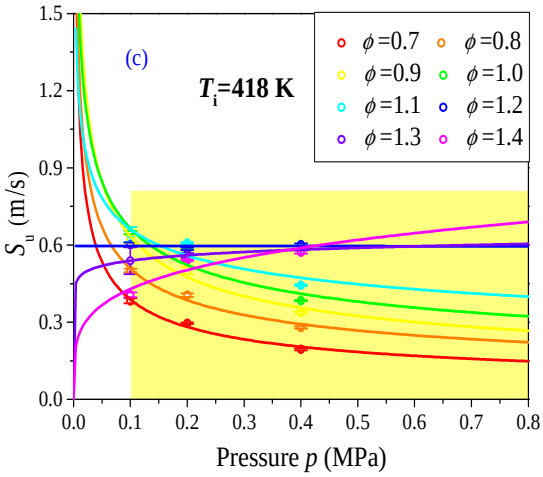

Figure 8. A graph of S_u versus p by extrapolation at the condition of: (a) T_i=358 K; (b) T_i=388 K; (c) T_i=418 K (The shadow area represents the research range of pressure in this paper).

5.4. S_u^0 as a function of temperature

Figure 9 shows the variation of S_u^0 as a function of T_u at three fixed pressures (0.1, 0.2 and 0.4 MPa). In Figure 9(b) and (c), the blue areas, on the left of the black lines, represent S_u^0 and the red areas on the right of the black lines, represent cellular flame speed. Black lines are at the intersection of solid lines and dotted lines. In Figure 9(b), the flame is cellular at ϕ=1.3 and the flame is laminar at ϕ=1.2; therefore, cellularity could appear between 1.2 and 1.3. Therefore, the black line lies between ϕ=1.2 and 1.3. In Figure 9(c), the black line is between ϕ=1.1 and 1.2. It can be seen from Figure 9 that S_u^0 increases with increasing temperature. It can also be observed that the shape of curves at the same pressure are similar, especially at p_i=0.2 MPa and p_i=0.4 MPa. Additionally, at the same pressure, the positions correspond to the maximum flame speed are similar. With the increase of pressure, the peak shifts right, from ϕ=1.0 to ϕ=1.3, which is also impacted by cellularity to some extent, because cellularity accelerates the flame speed at ϕ=1.2-1.4. Therefore, pressure has little influence on the shape of the curves and the station of the peak. It can also be found that cellularity appears at ϕ=1.3-1.4 when p_i=0.2 MPa and at ϕ=1.2-1.4 when p_i=0.4 MPa, which confirms cellularity has a strong relation with pressure. The larger the pressure, the earlier cellularity appears.

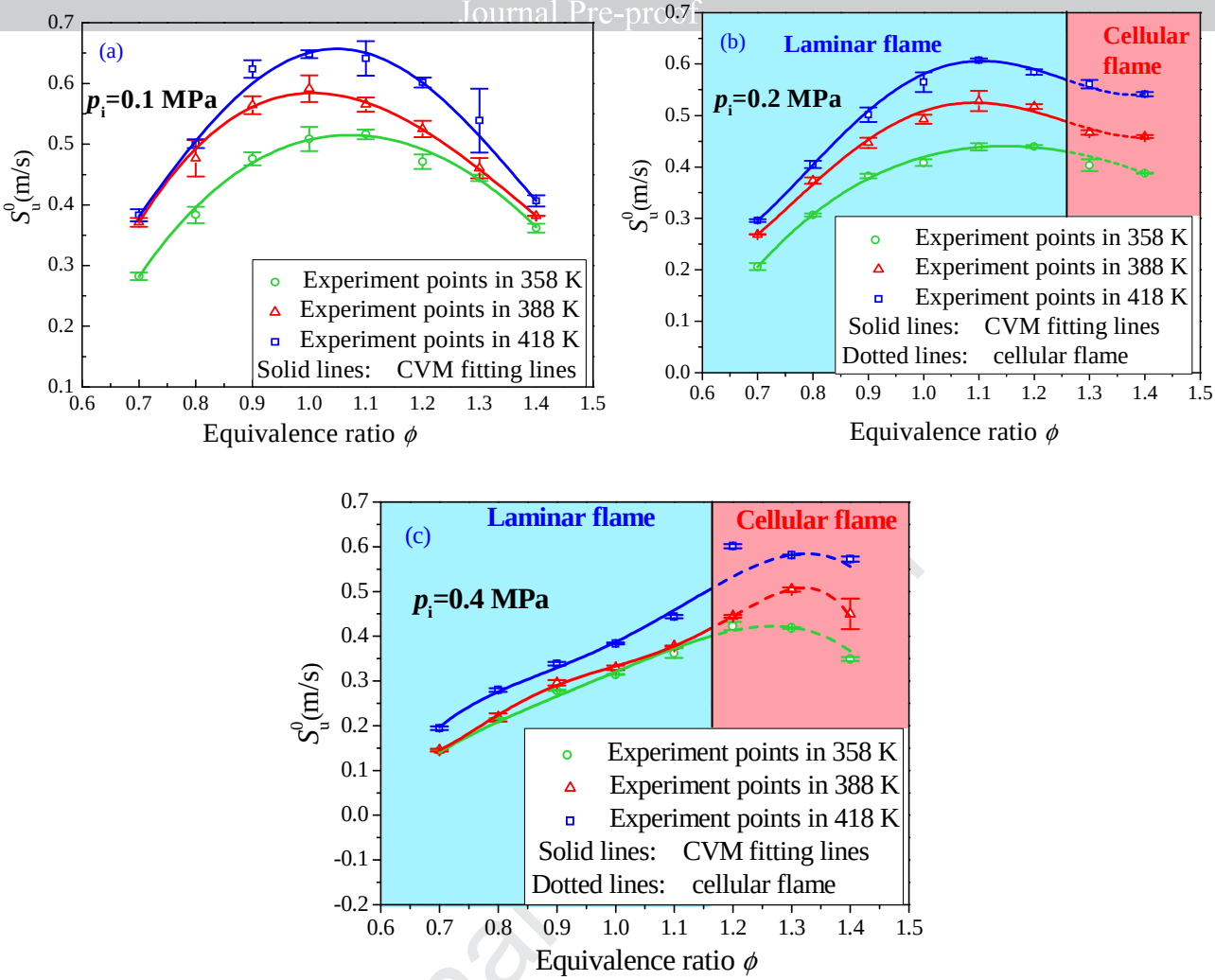

Figure 9. S_u^0 at T_i=358, 388 and 418 K: (a) p_i=0.1 MPa; (b) p_i=0.2 MPa; (c) p_i=0.4 MPa (Solid lines stand for S_u^0, while dotted lines stand for cellular flame speed. Blue areas represent S_u^0 and red areas represent cellular flame speed).

Figure 10 shows the variation of S_u as a function of T_u at ϕ= 0.7-1.4 and p_i=0.1, 0.2 and 0.4 MPa. The power law correlations fitted to three experimental data at T_i=358, 388 and 418 K respectively give a very good fit. According to the fitting zone referred in Section 4.1, the S_u could be obtained at T_i=490 K. It can be seen from Figure 10 that the S_u increases with an increase in temperature. And the increasing rate becomes faster and faster with an increase of temperature.

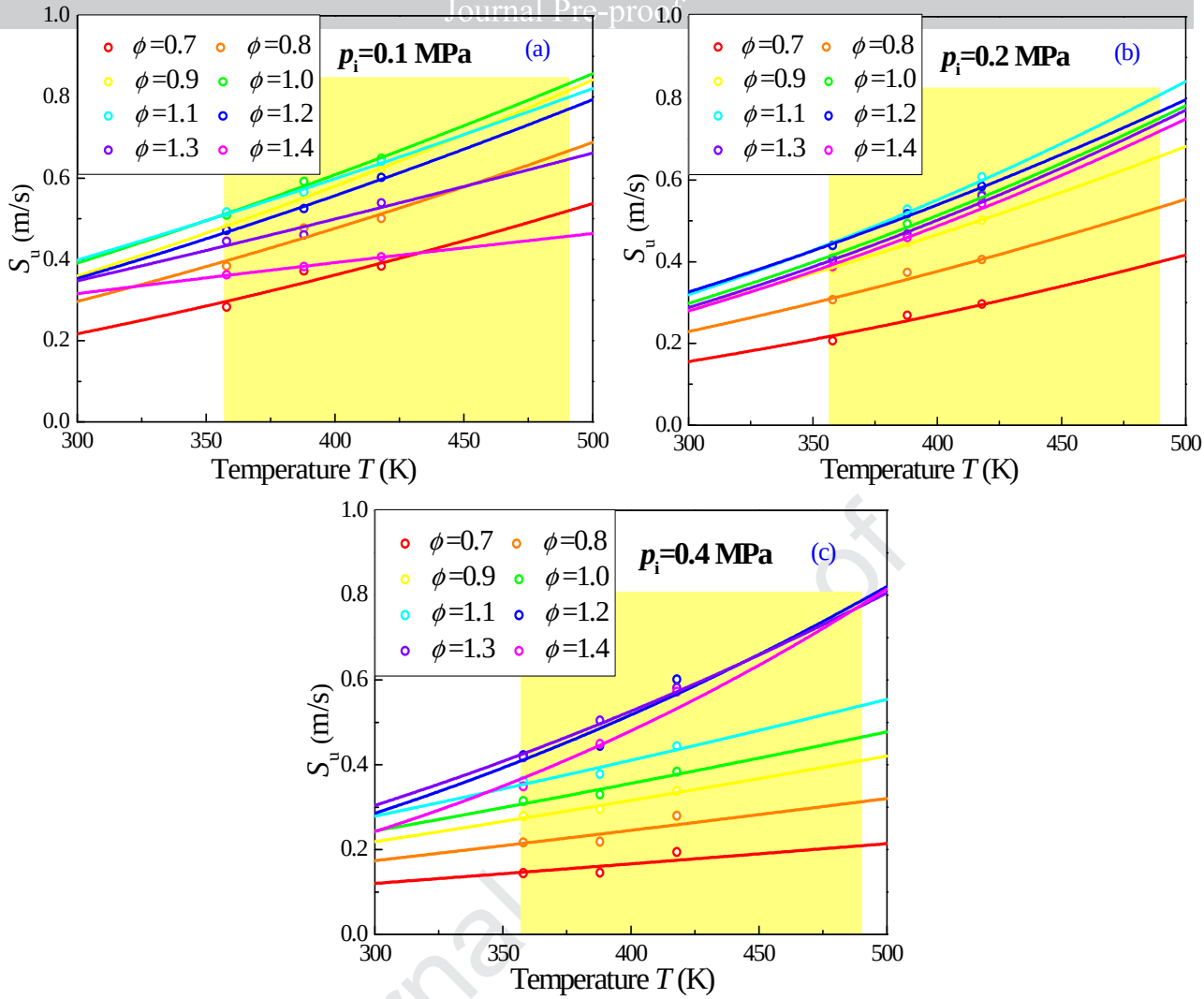

Figure 10. S_u as a function of T_u by extrapolation at the condition of (a) p_i=0.1 MPa; (b) p_i=0.2 MPa; (c) p_i=0.4 MPa. (The shadow area represents the research range of temperature in this paper).

5.5. S_u at elevated pressures and temperatures

Figure 11 shows S_u obtained at two initial pressures and temperatures conditions. In each experiment, S_u increased with pressure in a power law. Although the high pressure has a negative impact on S_u, increased the temperature during combustion offsets the negative impact of increased pressure on S_u. That is also the reason why in Figure 3 S_u increases at the early stage. As assumption (1), the procedure is isentropic and eq. (2) is used to calculate the temperature from pressure. Therefore, if both p/p_i and T_i (which decides k_u) are the same, temperature during the combustion procedure will be regarded as the same. The fitting lines fit well when p/p_i is from 1 to 2 in all figures, so in this paper, S_u in all experiments are intended to be chosen from initial conditions to the point, at which p/p_i is equal to 2. In Figure 11, there are only two figures at different conditions shown as representatives.

Another seven figures are similar to Figure 11, so they are not shown in this paper. In Figure 11(b), lines at ϕ=1.3-1.4 increase rapidly, which is caused by cellularity. The detailed explanation and figure can be seen in Figure 5.

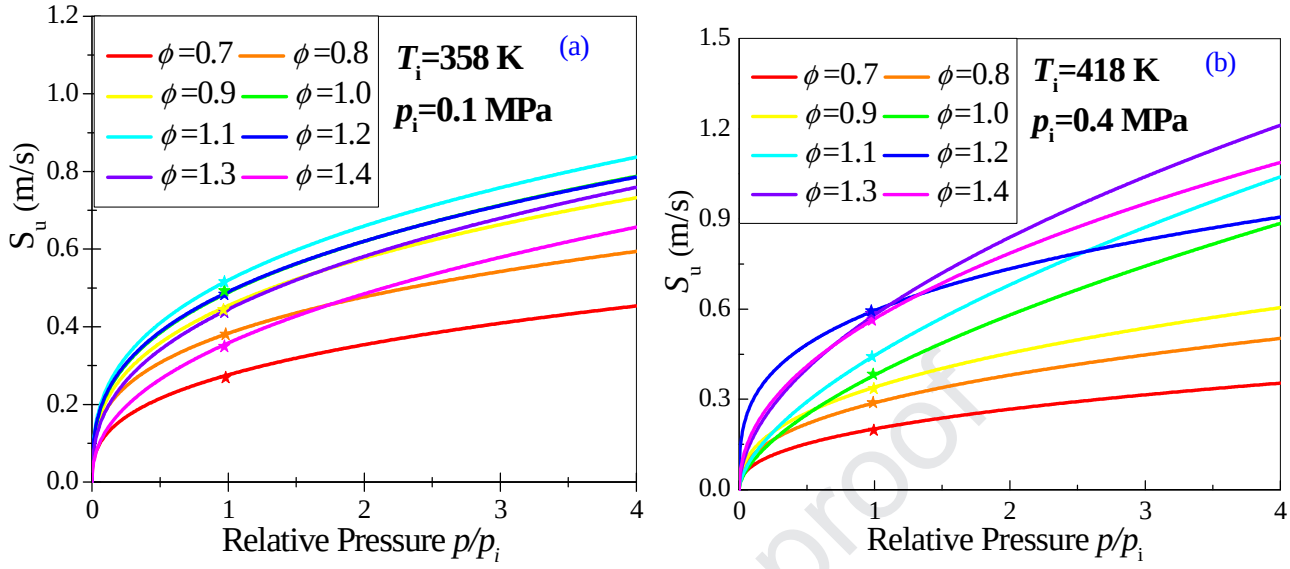

Figure 11. S_u as a function of p/p_i at ϕ=0.7-1.4: (a) p_i=0.1 MPa, T_i=358 K; (b) p_i=0.4 MPa, T_i=418 K.

5.6. Fitting correlation for S_u

Figure 12 shows the fitting ranges of p and T_u. There are 9 experimental points at every equivalence ratio. The fitting correlation given in this paper is valid at p_i= 0.1-0.8 MPa, T_i= 358-490 K and ϕ= 0.7-1.4. In the CVM, a series of S_u over a certain range of pressure and temperature were obtained from a single test. Therefore, starting with the initial (p_i,T_i) value, one can draw a continuous line of higher (p,T_u) values for which S_u can be determined from the fit. Then, interpolation and extrapolation methods were used to fill up the whole areas.

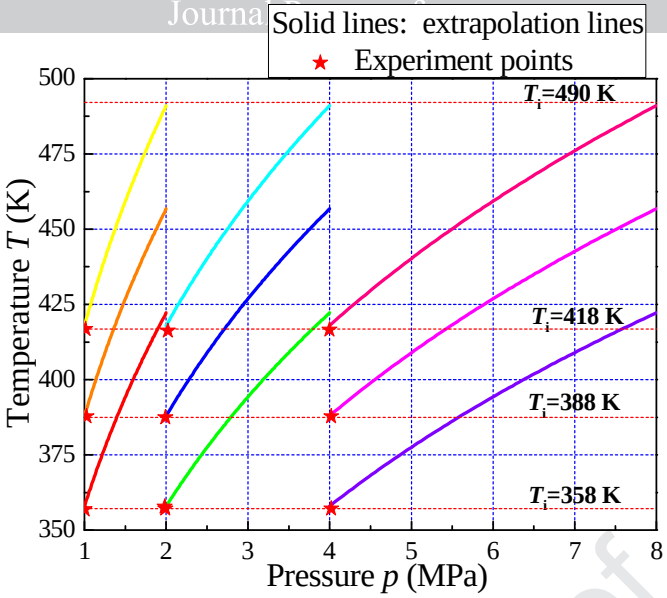

Figure 12. Range of fitting correlation (Colorful solid lines represent fitting lines in the CVM).

In all the experiments, the variation of S_u with p/p_i can be plotted like Figure 3. S_u from p/p_i =1 to p/p_i=2 was chosen. At last, an explicit correlation with fitted S_u as the function of p, T_u and ϕ can be obtained:

$$S_u = A(T/358)^{\alpha}(p/0.1)^{\beta} \tag{11}$$

where:

$$A = S_{u,0} + S_{u,1}(\phi-1) + S_{u,2}(\phi-1)^2 + S_{u,3}(\phi-1)^3 + S_{u,4}(\phi-1)^4$$

$$\alpha = \alpha_0 + \alpha_1(\phi-1) + \alpha_2(\phi-1)^2 + \alpha_3(\phi-1)^3$$

$$\beta = \beta_0 + \beta_1(\phi-1) + \beta_2(\phi-1)^2$$

Table 3 lists the values of the correlation coefficients. The values of A, α and β at various equivalence ratios can be seen in the Appendix. Figure 13 gives a comprehensive description about the effect of both T_u and p on S_u. It can be found that S_u increases with temperature, just like what Figure 10 shows, and S_u decreases with pressure, just like what Figure 8 shows. S_u increases from the zone that pressure is high and the temperature is low to the zone that pressure is low and the temperature is high. The maximum and average deviations between S_u from fitting correlation and S_u from experiments under p_i=0.1-0.4 MPa, T_i=358-418 K, ϕ=0.7-1.4 are 15% and 9%, respectively.

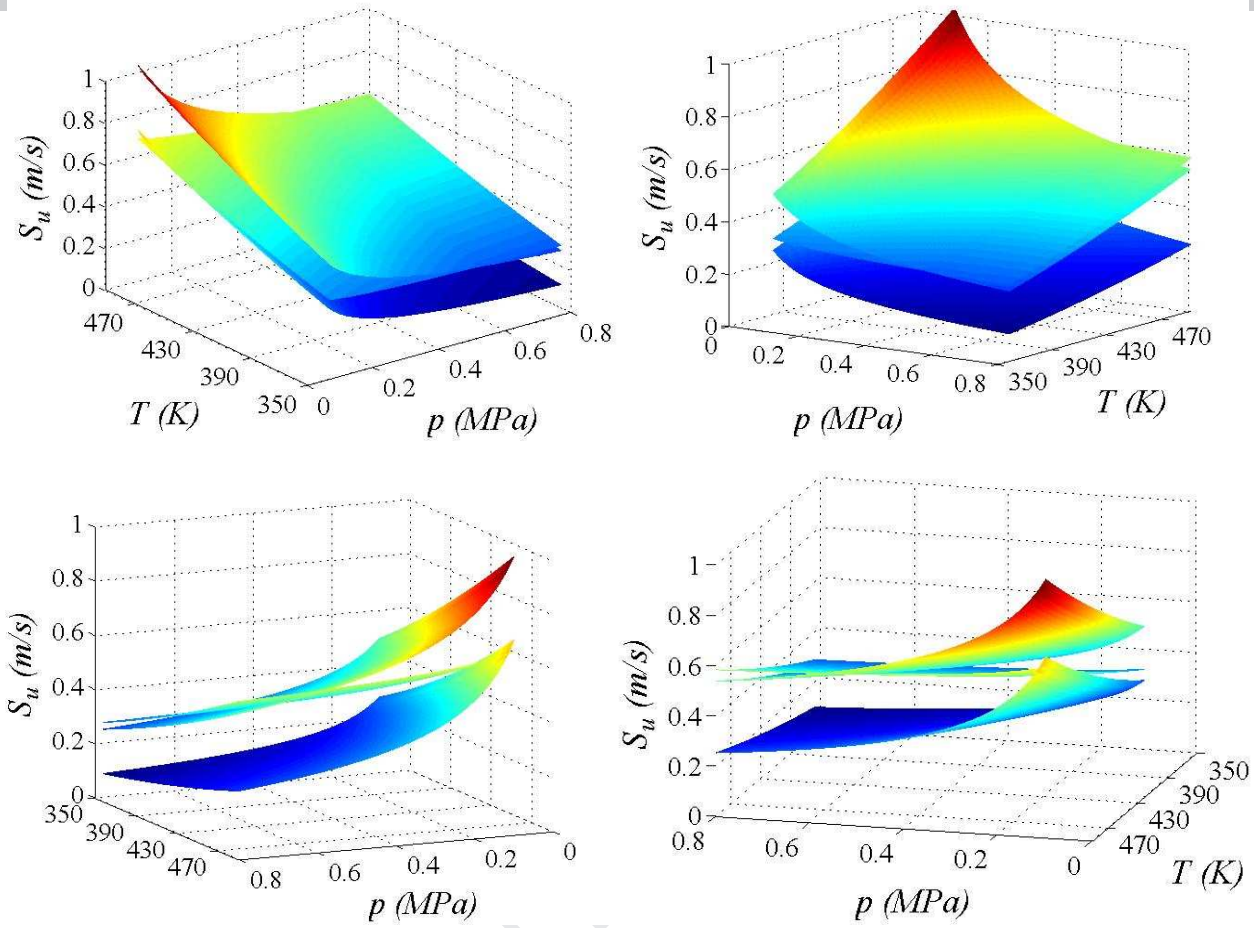

Figure 13. S_u as a function of p (0.1-0.8 MPa) and T_u (358-490 K) at ϕ= 0.7, 1, and 1.4 (four figures are the same but displayed in different observation angles)

Figure 14 shows A, α and β as the function of ϕ. It can be observed that fitting lines show a great agreement with points at all equivalence ratios.

Table 3 Correlation coefficients for mixed fuel

Parameter	Value
$S_{u,0}$	0.518
$S_{u,1}$	0.087
$S_{u,2}$	-1.955
$S_{u,3}$	1.084
$S_{u,4}$	1.161

α_0	2.068
α_1	-1.907
α_2	3.350
α_3	5.182
β_0	-0.290
β_1	0.843
β_2	0.196

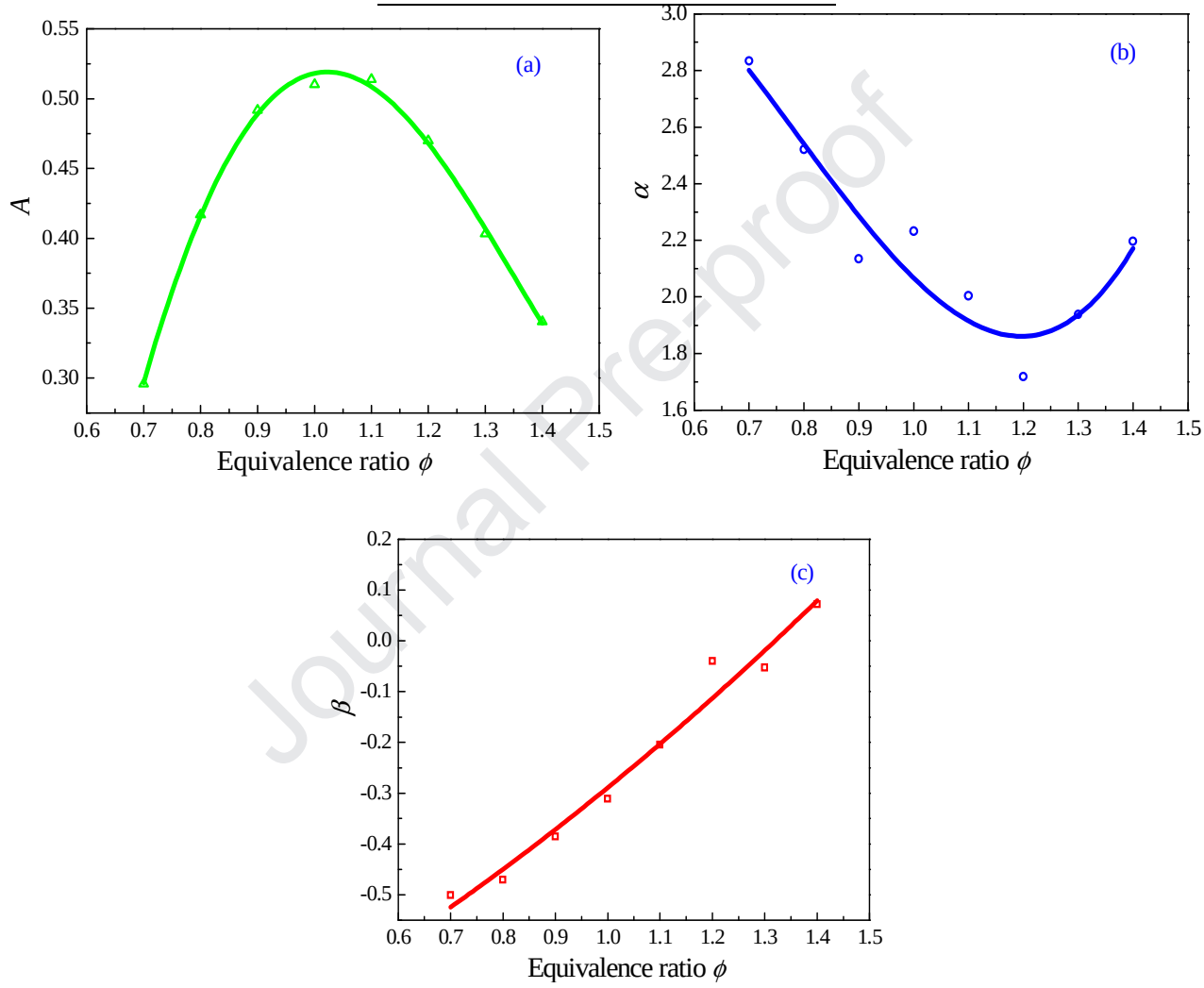

Figure 14. A, α and β as the function of ϕ

6 Conclusions

The burning speed of the fast pyrolysis fuel was tested in the CVCC at p_i=0.1-0.4 MPa, T_i=358-418 K, and ϕ=0.7-1.4. The CVM, which takes the combustion pressure trace as the main input, was used to determine S_u for conditions beyond the initial conditions (p to 0.8 MPa, T_u to 490 K). The CPM, which takes Schieren flame images as the main input, was also used to determine S_u. The S_u

results obtained from the CVM and CPM were compared. The main conclusions of this study are the following:

1. Discrepancies of S_u from the CVM and CPM are within 15%. The flame radius calculation in the CPM and the determination of the burned mass fraction in CVM are considered to contribute to the discrepancies in the paper.

2. Influences of temperature, pressure and equivalence ratio on S_u of the fast pyrolysis biofuel were identified. Compared with pressure, the impact of temperature on the value of S_u at most conditions is greater, so in a single experiment, with both temperature and pressure increase simultaneously, S_u tends to increases at the early stage of combustion. With increasing equivalence ratio, S_u increases first, peaks around ϕ=1.0-1.1 and then decreases except when cellularity appears.

3. An explicit 12-terms correlation for S_u as the function of pressure, temperature and equivalence ratio was obtained. This correlation is effective in determination of S_u in the boundary conditions of p=0.1-0.8 MPa pressure, T_u=358-490 K temperature and ϕ=0.7-1.4. The maximum and average deviations between S_u from fitting correlation and S_u from experiments under p_i=0.1-0.4 MPa, T_i=358-418 K, ϕ=0.7-1.4 are 16.2% and 7.3%, respectively.

4. Cellularity appears because of the flame instability at high pressure and temperature. It led to a significant increase in flame speed. Results show pressure contributes greatly to the appearance of cellularity.

Acknowledgements

Financially this study was funded by the National Natural Science Foundation of China (NO. 91741203 and 51336008), the Public Beneficial Technology Application Research Project of Science Technology Department of Zhejiang Province (NO. 2016C31102 and 2016C31112), the Fundamental Research Funds for the Central Universities of China (NO. 2013QNA4017), and the Hangzhou Science Committee (NO.20162013A06) of China.

Table S1 lists A, α and β at various equivalence ratios.

Table S1 A, α and β at various equivalence ratios

Parameter	A	α	β
0.7	0.30	2.83	-0.50
0.8	0.42	2.52	-0.47
0.9	0.49	2.14	-0.39
1.0	0.51	2.23	-0.31
1.1	0.51	2.00	-0.20
1.2	0.47	1.72	-0.04
1.3	0.40	1.94	-0.05
1.4	0.34	2.20	0.07

Reference

[1] Wang S, Dai G, Yang H, Luo Z. Lignocellulosic biomass pyrolysis mechanism: A state-of-the-art review. Prog Energy Combust Sci 2017;62:33-86.

[2] Luo Z, Wang S, Liao Y, Zhou J, Gu Y, Cen K. Research on biomass fast pyrolysis for liquid fuel. Biomass and Bioenergy 2004;26:455-462.

[3] Q. Dang, Luo Z, Zhang J, et al. Experimental study on bio-oil upgrading over Pt/SO24-/ZrO2/SBA-15 catalyst in supercritical ethanol. Fuel 2013;103:683-692.

[4] Xu C, Zhong A, Li X, Wang C, Sahu A, Xu H, et al. Laminar burning characteristics of upgraded biomass pyrolysis fuel derived from rice husk at elevated pressures and temperatures. Fuel 2017;210:249-261.

[5] Varea E, Beeckmann J, Pitsch H, Chen Z, Renou B. Determination of burning velocities from spherically expanding H_2/air flames. P Combust Inst 2015;35:711-719.

[6] Beeckmann J, Hesse R, Kruse S, Berens A, Peters N, Pitsch H, et al. Propagation speed and stability of spherically expanding hydrogen/air flames: Experimental study and asymptotics. P Combust Inst 2017;36:1531-1538.

[7] Burke MP, Chen Z, Ju Y, Dryer FL. Effect of cylindrical confinement on the determination of laminar flame speeds using outwardly propagating flames. Combust Flame 2009;156:771-779.

[8] Chen Z. On the extraction of laminar flame speed and Markstein length from outwardly propagating spherical flames. Combust Flame 2011;158:291-300.

[9] Chen Z, Burke MP, Ju Y. Effects of compression and stretch on the determination of laminar flame speeds using propagating spherical flames. Combust Theory Model 2009;13:343-364.

[10] Faghih M, Chen Z. The constant-volume propagating spherical flame method for laminar flame speed measurement. Sci Bull 2016;61:1296-1310.

[11] Hu X, Yu Q. Effect of the elevated initial temperature on the laminar flame speeds of oxy-methane. Energy 2018;147:876-883.

[12] Zeng W, Liu J, Ma H, Liu Y, Liu A. Experimental study on the flame propagation and laminar combustion characteristics of landfill gas. Energy 2018;158:437-448.

[13] Lee S, Ha H, Dunn-Rankin D, Kwon OC. Effects of pressure on structure and extinction limits of counterflow nonpremixed water-laden methane/air flames. Energy 2017;134:545-553.

[14] Ku J, Choi D, Kim H, Lee S, Kwon OC. Extinction limits and structure of counterflow nonpremixed methane-ammonia/air flames. Energy 2018;165:314-325.

[15] Tang A, Cai T, Deng J, Zhao D, Huang Q, Zhou C. Experimental study on flame structure transitions of premixed propane/air in micro-scale planar combustors. Energy 2019;179:558-570

[16] Wan J, Fan A, Yao H, Liu W. Experimental investigation and numerical analysis on the blow-off limits of premixed CH_4/air flames in a mesoscale bluff-body combustor. Energy

[17] Fan A, Zhang H, Wan J. Numerical investigation on flame blow-off limit of a novel microscale Swiss-roll combustor with a bluff-body. Energy 2017;123:252-259.

[18] Xiouris C, Ye T, Jayachandran J, Egolfopoulos FN. Laminar flame speeds under engine-relevant conditions: Uncertainty quantification and minimization in spherically expanding flame experiments. Combust Flame 2016;163:270-283.

[19] Hu E, Huang Z, He J, Miao H. Experimental and numerical study on laminar burning velocities and flame instabilities of hydrogen–air mixtures at elevated pressures and temperatures. Int J Hydrogen Energy 2009;34:8741-8755.

[20] Tang C, Huang Z, Jin C, He J, Wang J, Wang X, Miao H. Laminar burning velocities and combustion characteristics of propane–hydrogen–air premixed flames. Int J Hydrogen Energy 2008;33:4906-4914.

[21] Chen Z. On the accuracy of laminar flame speeds measured from outwardly propagating spherical flames: Methane/air at normal temperature and pressure. Combust Flame 2015;162:2442-2453.

[22] Wu X, Huang Z, Wang X, Jin C, Tang C, Wei L, Law CK. Laminar burning velocities and flame instabilities of 2,5-dimethylfuran–air mixtures at elevated pressures. Combust Flame 2011;158:539-546.

[23] Ai Y, Zhou Z, Chen Z, Kong W. Laminar flame speed and Markstein length of syngas at normal and elevated pressures and temperatures. Fuel 2014;137:339-345.

[24] Sun ZY, Li GX. Propagation speed of wrinkled premixed flames within stoichiometric hydrogen-air mixtures under standard temperature and pressure. Korean J Chem Eng 2017;34:1846-1857.

[25] Chen Z. Effects of radiation absorption on spherical flame propagation and radiation-induced uncertainty in laminar flame speed measurement. Proc Combust Inst 2017;36:1129-1136.

[26] Ellis OCDC. Flame movement in gaseous explosive mixtures. Fuel 1928;7:245-252.

[27] Lewis B, Elbe GV. Determination of the Speed of Flames and the Temperature Distribution in a Spherical Bomb from Time - Pressure Explosion Records. J Chem Phys 1934;2:283-290.

[28] Rallis CJ, Garforth AM. The determination of laminar burning velocity. Prog Energy Combust Sci 1980;4:303-329.

[29] Askari O, Elia M, Ferrari M, Metghalchi H. Cell formation effects on the burning speeds and flame front area of synthetic gas at high pressures and temperatures. Applied Energy 2017;189:568-577.

[30] O'Donovan KH, Rallis CJ. A modified analysis for the determination of the burning velocity of a gas mixture in a spherical constant volume combustion vessel. Combust Flame 1959;3:201-214.

[31] Saeed K, Stone CR. Measurements of the laminar burning velocity for mixtures of methanol and

air from a constant-volume vessel using a multizone model. Combust Flame 2004;139:152-166.

[32] Saeed K, Stone CR. The modelling of premixed laminar combustion in a closed vessel. Combustion Theory and Modeling 2004;8:721-743.

[33] Luijten CCM, Doosje E, Goey LPHD. Accurate analytical models for fractional pressure rise in constant volume combustion. Int J Thermal Sci 2009;48:1213-1222.

[34] Luijten CCM, Doosje E, Oijen JAV, Goey LPHD. Impact of dissociation and end pressure on determination of laminar burning velocities in constant volume combustion. Int J Thermal Sci 2009;48:1206-1212.

[35] Chen Z, Burke MP, Ju Y. Effects of Lewis number and ignition energy on the determination of laminar flame speed using propagating spherical flames. Proc Combust Inst 2009;32:1253-1260.

[36] Chen Z. Effects of radiation and compression on propagating spherical flames of methane/air mixtures near the lean flammability limit. Combust Flame 2010;157:2267-2276.

[37] Huang Z, Zhang Y, Zeng K, Liu B, Wang Q, Jiang D. Measurements of laminar burning velocities for natural gas–hydrogen–air mixtures. Transactions of Csice 2006;146:302-311.

[38] Huang Z, Wang Q, Yu J, Zhang Y, Zeng K, Miao H, et al. Measurement of laminar burning velocity of dimethyl ether–air premixed mixtures. Fuel 2007;86:2360-2366.

[39] Zhang X, Huang Z, Zhang Z, Zheng J, Yu W, Jiang D. Measurements of laminar burning velocities and flame stability analysis for dissociated methanol–air–diluent mixtures at elevated temperatures and pressures. Int J Hydrogen Energy 2009;34:4862-4875.

[40] Hinton N, Stone R, Cracknell R. Laminar burning velocity measurements in constant volume vessels–Reconciliation of flame front imaging and pressure rise methods. Fuel 2018;211:446-457.

[41] Hinton N, Stone R, Cracknell R, Olm C. Aqueous ethanol laminar burning velocity measurements using constant volume bomb methods. Fuel 2018;214:127-134.

[42] Xu C, Fang D, Luo Q, Ma J, Xie Y. A comparative study of laser ignition and spark ignition with gasoline–air mixtures. Optics and Laser Technology 2014;64:343-351.

[43] Xu C, Fang D, Luo Q, Ma J, Xie Y, Zheng X. Characterization of gasoline combustion with laser and spark ignition. Journal of Zhejiang University-SCIENCE A 2015;16:830-838.

[44] Xu C, Hu Y, Li X, Zhou X, Zhong A. Comparative experimental study of ethanol-air premixed laminar combustion characteristics by laser induced spark and electric spark ignition. Korean J Chem Eng 2017;34:574-579.

[45] Omari A, Tartakovsky L. Measurement of the laminar burning velocity using the confined and unconfined spherical flame methods–A comparative analysis. Combust Flame 2016;168:127-137.

[46] Reyes M, Tinaut FV, Horrillo A, Lafuente A. Experimental characterization of burning velocities of premixed methane-air and hydrogen-air mixtures in a constant volume combustion bomb at moderate pressure and temperature. Appl Therm Eng 2018;130:684-697.

Research Highlights

1. Influences of T, P and ϕ on Su were evaluated for a pyrolysis fuel
2. Laminar burning speeds (Su) determined by CVM were compared with those by CPM.
3. CVM interprets Su over a larger pressure and temperature range than initial conditions.
4. An explicit correlation of Su was obtained from experimental results.
5. Cellular burning speed was calculated.